Lab on a Chip

PAPER

View Article Online
View Journal | View Issue



Cite this: *Lab Chip*, 2020, **20**, 3938

# Reduction of Taylor–Aris dispersion by lateral mixing for chromatographic applications†

Eiko Y. Westerbeek, [ab] Johan G. Bomer,[b] Wouter Olthuis, [b] Jan C. T. Eijkel[b] and Wim De Malsche *[a]

Received 30th July 2020,
Accepted 22nd September 2020

DOI: 10.1039/d0lc00773k

rsc.li/loc

Chromatographic columns are suffering from Taylor–Aris dispersion, especially for slowly diffusing molecules such as proteins. Since downscaling the channel size to reduce Taylor–Aris dispersion meets fundamental pressure limitations, new strategies are needed to further improve chromatography beyond its current limits. In this work we demonstrate a method to reduce Taylor–Aris dispersion by lateral mixing in a newly designed silicon AC-electroosmotic flow mixer. We obtained a reduction in $\kappa_{aris}$ by a factor of three in a 40 μm × 20 μm microchannel, corresponding to a plate height gain of 2 to 3 under unretained conditions at low to high Pe values. We also demonstrate an improvement of a reverse-phase chromatographic separation of coumarins.

## Introduction

The interplay between convection and diffusion steers the trajectory of a tracer particle in a flow environment. When several particles or molecules of the same species are simultaneously introduced in a channel with axial Poiseuille flow, variations in trajectories will result in an axial concentration distribution (Fig. 1). This phenomenon was first quantified in 1953 by Taylor for high Peclet numbers ($Pe = Ud/D_m \gg 1$, with $U$, the linear axial velocity, $d$ the characteristic cross-sectional dimension and $D_m$, the molecular diffusion coefficient). Later this theory was generalized in 1956 by Aris for all Peclet numbers, and is commonly referred to as Taylor–Aris dispersion.[1,2] The unavoidable occurrence of broadening of an introduced band results in a large loss of the performance of analytical flow devices where sample bands are to be analyzed. This sets a boundary on the attainable performance of kinetic separation devices, but also *e.g.* of continuous flow reactors.

Liquid chromatography is a well-known analytical technique suffering from Taylor–Aris dispersion. In liquid chromatography a sample band containing several species is injected into a column and separated into different bands, as a result of selective interaction of the species with the stationary phase. In chromatographic practice it is preferred to operate the system at as high as possible flow rates, to reduce the analysis time. Unfortunately, high velocities lead to excessive Taylor–Aris dispersion, resulting in axially elongated sample bands with dramatically reduced concentrations.

In the field of chromatography, dispersion is usually quantified by the dimensionless theoretical plate height,[3] which is the increase in band variance resulting from transport through the channel over a distance $\Delta x$:

$$h = \frac{1}{d}\frac{\Delta {\sigma_x}^2}{\Delta x} = \frac{2}{Pe} + 2{\cdot}\kappa_{aris}{\cdot}Pe \quad (1)$$

${\Delta\sigma_x}^2$ is the increase in variance of the solute concentration distribution between two axial positions separated by a length $\Delta x$. $\kappa_{aris}$ is a dimensionless number, which is determined by the differences in axial velocity across the channel cross section and the ability of a solute particle to transfer between different axial velocities. Together with the Peclet number, $\kappa_{aris}$ determines the efficiency of the chromatographic column. This equation shows that there is an optimum axial velocity at which the plate height is at its minimum. The

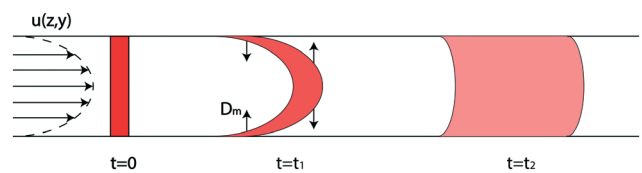


**Fig. 1** Taylor–Aris dispersion. A Poiseuille flow leads to the broadening of an injected band over time. The amount of Taylor–Aris dispersion results from the interplay between the transport of solute in axial and lateral direction. $t = 0$ shows the solute immediately after injection, $t = t_1$ displays the initial broadening with diffusion in the lateral direction as displayed by the arrows pointing up and down. $t = t_2$ displays broadening of the plug further down in the channel.

[a] *μFlow Group, Department of Chemical Engineering, Vrije Universiteit Brussel, Pleinlaan 2, 1050, Brussels, Belgium. E-mail: Wim.De.Malsche@vub.be*
[b] *BIOS Lab on a Chip Group, MESA+ Institute for Nanotechnology & Max Planck Centre for Complex Fluid Dynamics, University of Twente, Enschede 7500 AE, The Netherlands*

† Electronic supplementary information (ESI) available. See DOI: 10.1039/d0lc00773k

term, 2/Pe increases when Pe (and hence linear velocity) decreases while $2{\cdot}\kappa_{aris}{\cdot}Pe$ increases when Pe increases. In chromatography this equation is known as the van Deemter equation[4] (for a straight channel) (see *e.g.* Fig. 5c).

Below the optimal velocity, dispersion is dominated by the axial diffusion, while at higher velocities dispersion is dominated by Taylor–Aris dispersion. As a result, slowly diffusing species like proteins, nanoparticles, macromolecules and polymers, suffer most from Taylor–Aris dispersion.[5–7] This sets a fundamental limit on the performance of chromatographic and more general of all laminar flow devices where band broadening and dispersion are to be minimized.

In order to increase the sample loadability of chromatographic devices, they are commonly packed with particles or monolithic polymeric or silica materials. This results in a velocity independent dispersive term (so called A-term or eddy dispersion, a term that then appears in eqn (1)) as a result of heterogeneity of the stationary phase. When the stationary phase has a sufficiently high degree of order, with in the most ordered case a single open tubular channel, eddy dispersion vanishes. Improvements in performance of chromatographic formats have been realized by improving the order of particle beds, with as an extreme case ordered pillar array columns.[8–10] When extended in the lateral direction, they interestingly behave as a homogenous array of open tubular columns with undetectable variation in band mobilities between the parallel but still interconnected flow paths that are present to account for minimal variations in permeability.

During the past 50 years, most efforts to reduce plate height have been devoted to reducing $d$. In packed bed columns, $d$ is defined as the particle diameter, since the particle size determines the flow-through area. This reduction of $d$ leads to a reduction in the plate height, $H = d{\cdot}h$ and hence increases the absolute chromatographic performance. This development finally resulted in packed beds with particles as small as 1 μm. Difficulties in packing and excessive pressure drops, as well as the resulting viscous heating and concomitant temperature gradients however set a limit to this approach to further reduce dispersion. It is also important to note that pressure limitations impose constraints on the achievable chromatographic performance, which is tightly linked to the particle (or pillar) size.[11] The total attainable separation quality, often expressed as plate number ($N = L/(d{\cdot}H)$), increases as $d$ decreases. However, when $d$ decreases for a given channel length, the pressure that is needed to operate the channel at optimal conditions increases and becomes eventually limiting at the pressure limit of the system (*e.g.* 1000 bar). A reduction of particle size allows to reduce the separation time for less complex mixtures, but reduces the ability to separate more complex mixtures (which require longer separation times).[12] This tight coupling between dispersion and flow permeability sets a huge restriction on the chromatographic operation, which can possibly be relaxed when moving to new flow geometries or flow induction modes.

In conceiving approaches to further reduce the plate height of chromatographic columns, we can aim at minimizing the $\kappa_{aris}$ value in eqn (1) instead of $d$. When reducing $\kappa_{aris}$, the linear term $2{\cdot}\kappa_{aris}{\cdot}Pe$ increases less with increasing elution velocity and therefore the optimal elution velocity is shifting towards higher velocities. This also decreases the contribution of the 2/Pe term. The reduction of $\kappa_{aris}$ has been attempted in laminar flow systems in several ways. It can be realized in a passive way, by geometrically shaping the channel cross-section to render the axial flow velocity as uniform as possible across the channel cross section.[4] The presence of side walls in a rectangular channel increases $\kappa_{aris}$ with increasing aspect ratio and reaches a maximal value at high aspect ratio, being 8 times higher than the $\kappa_{aris}$ value that is obtained in a flow configuration composed of 2 parallel plates without side walls.[13] By locally providing deeper channels near the lateral wall region, $\kappa_{aris}$ can be brought close to a value of 1, *i.e.* mimicking the situation where no lateral walls are present.[14] Instead of uniformizing the axial flows, Stroock *et al.* pursued a strategy to induced a chaotic flow in 70 μm × 200 μm channels to disturb the Poiseuille flow, by providing 15 μm deep bas-relief grooves (staggered herringbone type) near a channel wall. This resulted in visible reduction in band broadening.[15] A limitation of this passive approach is that the chaotic nature of the induced mixing results in new dispersive sources. The induced mixing has a lateral degree of disorder and furthermore the formed eddies also have an axial component. Both are dispersive sources that will dominate when the system is further scaled down when attempting to further increase performance. Furthermore, scaling down the herringbone mixer will cause difficulties in manufacturing, since the grooves are small compared to the channel size. When scaling down the channels to several μm, the grooves will become smaller than the limits of standard lithography set-ups, and flow will furthermore cease at such small groove dimensions. Downscaling of channel dimensions is however imperative because one needs to compete with absolute performance values, for which sub-micron (spacing between packing structures) dimensions are needed for the highest-end chromatographic separations. Also in the context of continuous flow reactors, small dimensions below 1 mm down to a few tens of μm are desired. Small dimensions are wanted because large surface-to-volume ratios allow for a large specific surface needed for depositing catalysts, which maximizes the rates of reactions.[16]

Reducing $\kappa_{aris}$ by inducing turbulence is another approach that can be envisioned. An overview of several attempts to reduce $\kappa_{aris}$ is provided in Table 1. When low (kinematic) viscosity ($\eta$) fluids are handled in unstructured channels at high linear velocities ($U$) with large characteristic dimensions ($d$), the natural transition towards turbulent flow will assist in reducing Taylor–Aris dispersion. However, at common values used in liquid microflow systems where Taylor–Aris dispersion is a problem to be avoided, including chromatographic separation systems, Re values remain within the Stokes regime ($Re = Ud/\eta < 1$) with a well-defined laminar flow. In gas phase systems on the other hand, turbulence-induced reduction in Taylor–Aris dispersion has been effectively demonstrated in the context of gas chromatography.[17] A

Table 1 Strategies to reduce Taylor–Aris dispersion by lateral mixing, pursued so far

| Ref. | Characteristic channel dimension ($d$) | Medium | Mixing technique | Reduction in $\kappa_{aris}$ |
|---|---|---|---|---|
| 15 | 200 μm | Liquid | Passive mixing | Not investigated |
| 17 | 380 μm | Gas | Turbulence | 95% |
| 18 | 1 mm | Liquid | Magnetic beads | 80% |

performance gain could however only be observed at non-optimal conditions, *i.e.* at very high flow rates leading to reference performance values that are more than an order of magnitude larger than what would be achieved under ideal reference conditions. It can therefore be concluded that all presently available passive approaches fail in improving the absolute performance of techniques suffering from Taylor–Aris dispersion.

We can also decrease $\kappa_{aris}$ by actively generating flow in the lateral direction, orthogonal to the axial pressure gradient. In order to reduce dispersion in devices operated at optimal conditions, using lateral flow, the lateral flow needs then to be uniformly distributed, should lack or have a minimal axial component and ideally needs to be scalable to submicron channel dimensions. To meet these requirements, a lateral flow driving mechanism orthogonal to the pressure driven flow should be applied. A number of methods are available for this aim. When introducing an ideal lateral vortex flow over the entire channel boundary, fluid dynamics simulations in square channels (aspect ratio 1) have indicated that dispersion can be theoretically reduced even below the dispersion between 2 infinite parallel plates.[19]

By magnetically actuating magnetic particles of sufficiently large size, the flow around these particles can be locally disturbed, therewith flattening the Poiseuille profile.[18] A reduction of $\kappa_{aris}$ by a factor of 5 was experimentally demonstrated using magnetic nanoparticles ($d$ = 25 nm) in a rotating magnetic field configuration in a cylindrical tube with the large diameter of 1 mm. The need for including 0.1–1% solid load of nanoparticles and the large tube size with an inherently large Taylor dispersion (even after a 5-fold reduction), as well as the problematic scalability, seem to limit practical implementation of this technique in fluidic and chromatographic applications.

Acoustic streaming is an example of a method to generate long-range lateral flow, but unfortunately also has limited downscaling potential.[20,21] In order to achieve bulk streaming in this case, the channel width $w$ should be matched to the wavelength ($\lambda$) of the used pressure wave ($w = n\lambda/2$, with $n$ an integer). For a standard commercially available piezo element with a frequency of 10 MHz, the channel size is limited to about 75 μm in an aqueous solution ($v_{aq}$ = 1500 m s$^{-1}$), which is too large for many applications. Furthermore, acoustic streaming generally has, apart from the lateral component, also a periodical axial component, which would limit the attainable gain.[22]

Here we propose to impose a laterally oriented electroosmotic flow (EOF). Axially oriented DC-EOF was developed in the 90s and is highly appreciated in the microfluidic community for its dispersion-limiting plug flow profile resulting from the slip boundary condition.[23] However, its application for liquid chromatography (capillary electrochromatography) never fulfilled its promise and did not lead to a breakthrough.[24] The main reasons are restrictions of the attainable liquid phase velocity at commercial voltage maxima (25 kV), the compulsory use of insulating substrates (excluding all metals), the competing requirements of the chemical nature of the channel surface to sustain EOF on the one hand (requiring free charge carriers on which an electrical double layer can form) and the need for an appropriate chemical environment for the chemical application on the other hand (*e.g.* interaction with a chromatographic coating or with a catalyst), again often conflicting with the optimal conditions for the actual separation application.[25] In contrast to DC-EOF, in AC-EOF a periodically induced charge above conducting electrodes takes over the role of the permanent charge on the channel walls.[26] As the electrode configuration can be chosen freely, it is in concept possible to produce the lateral flow required to reduce Taylor–Aris dispersion. As the electrodes can be placed at a distance in the μm range, high electrical fields and concomitantly considerable induced flow velocities can be generated.

In the present contribution, we exploit laterally induced AC-EOF flows superimposed on an axial pressure-driven flow as an approach to suppress Taylor–Aris dispersion. Importantly, this technique is scalable to dimensions that are relevant for chromatography. Key is furthermore the implementation of a novel out-of-plane configuration in silicon, encompassing the entire fluidic channel in a laterally uniform way and allowing to achieve purely anisotropic vortices without an axial component.[27] While this concept has a large potential to dramatically improve liquid chromatography practices, we anticipate that this development also gives the prospect to reduce dispersion at relevant dimensions for flow systems in general, allowing to *e.g.* drastically increase the performance of analytical separations devices.

## Materials & methods

### Chip fabrication

Fig. 2 schematically shows the entire manufacturing process. The substrate used for the chip design, is a p++ SOI wafer with a 10 μm device layer and a 1 μm buried oxide layer supplied by Siegert Wafer. The wafers were first thermally oxidized (300 nm) to have a hard mask for dry etching. Next, standard photolithography with resist type Olin 907-35 was used to define a channel. The channel was plasma etched

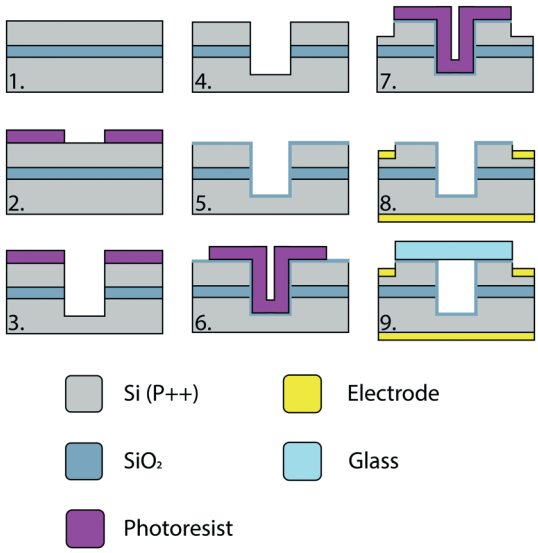


**Fig. 2** Manufacturing process of the chip 1. P++ SOI wafer as a substrate. 2. Standard lithography 3. dry etching of the channel. 4. Stripping of photoresist 5. thermal oxidation of silicon. 6. Spray-coating of photoresist and lithography. 7. Dry etching electrode pads. 8. Sputtering of Ti/Pt layer and lift-off. 9. Anodic bonding of borosilicate glass to the patterned Si substrate.

through the hard mask, device layer, buried oxide layer and finally 10 μm into the handle layer. The left-over resist was stripped in oxygen plasma (Tepla360). A thermal oxidation step was performed to grow a 13 nm oxide layer for isolation of the channel. To make the electrodes accessible, 5 μm deep trenches in the device layer were etched. The electrodes were fabricated by sputter deposition of 10 nm titanium and 200 nm platinum. A standard photolithographic resist mask served as etch mask and subsequent lift-off mask. A Borosilicate glass wafer (MEMpax®) was anodically bonded on the top of the wafer, using 1000 V at 400 °C (EVG510). Finally, the wafer was diced into chips (Loadpoint Micro Ace 3). The chip was connected to fluidic tubing with a side connect chip holder (Micronit). The etching of the silicon oxide hard mask, the buried oxide layer and the isolation layer was performed using a PlasmaTherm 790 plasma etcher, while for the etching of silicon an Oxford Instruments PlasmaPro 100 Estrellas was used. A picture of the chip in its microfluidic chip holder can be observed in Fig. S1.†

### Chip coating

The coating of the chip was performed by connecting the chip by silica capillaries to a bottle with solvent which was pressurized with nitrogen (~2 bar). The different solvents were flushed through the chip using the scheme provided in the ESI† (Table S1).

### Particle tracking

For the flow visualization experiments, a $KNO_3$ solution (0.1 mM) was used with fluorescent 500 nm melamine resin particles (Microparticle Gmbh). The chip was connected to a function generator as voltage source (Keysight 33500B). The microscope used was a DMI5000 (Leica) with a PE-300 Ultralight (CoolLed) and a CMOS camera (Hamamatsu). The channel was filled with the particle electrolyte solution, after which the AC-potential was turned on. The captured images where analyzed using General Defocusing Particle Tracking software.[28]

### Dispersion & separation experiments

An uncoated chip was connected to 4 Flow EZ Fluigent microfluidic pumps. The electrolyte used was a 0.1 mM $KNO_3$ solution with 50 μM FITC-dextran 20 kDa (Sigma Aldrich). The microscope used was a Leica DMi8 with a mercury lamp (Leica) and an CCD camera (Hamamatsu C13440). An AC-potential was applied using a function generator (Keysight 33500B). The intensity of the fluorescence signal over time was determined at two positions, by reading out a row of pixels over the width of the channel and determining the average intensity in time using ImageJ. The temporal concentration profile was then plotted and fitted with a Gaussian distribution using Origin 2019. Separation experiments were performed using the same set-up as for the dispersion experiments, but with a C18 coated chip. For the eluent, 70/30 (v/v%) water/methanol was used with a solution with 0.1 mM $KNO_3$ and 50 μM of both coumarin 440 and coumarin 480 (Sigma Aldrich).

## Results & discussion

### Electrochemical considerations and electrode design

To induce the desired lateral mixing by AC-EOF for the reduction of the Taylor–Aris dispersion, an electrode configuration was designed and integrated in silicon (Fig. 3b).

In AC-EOF, the electrodes operate in induced charge (IC) mode at appropriate AC frequencies, whereby at any given moment the applied electrical field and the counterionic charge have opposite signs. This results in an oscillating unidirectional flow, with a magnitude that depends on the actuation frequency. AC-electroosmotic slip flow is often described by the time dependent Helmholtz–Smoluchowski equation, which states:

$$u(t) = -\frac{\varepsilon}{\eta}\Delta\phi_{\mathrm{d}}(t)E_{\mathrm{t}}(t) \quad (2)$$

with $\varepsilon$ the permittivity, $\eta$ the viscosity, $\Delta\phi_{\mathrm{d}}$ the potential drop over the diffuse part of the double layer and $E_{\mathrm{t}}$ the electric field tangential to the slip-surface. In AC-EOF both the potential over the double layer and the electric field will vary in time. Green *et al.* adapted this equation to determine the average velocity over an AC-cycle.[29]

AC-EOF is mainly used to generate axial flow in microfluidic channels, whereby generally metal electrodes are used that are in direct contact with the solution (Fig. 3a). This direct contact of the metal electrode with the solution however is less desirable, as solution components can be

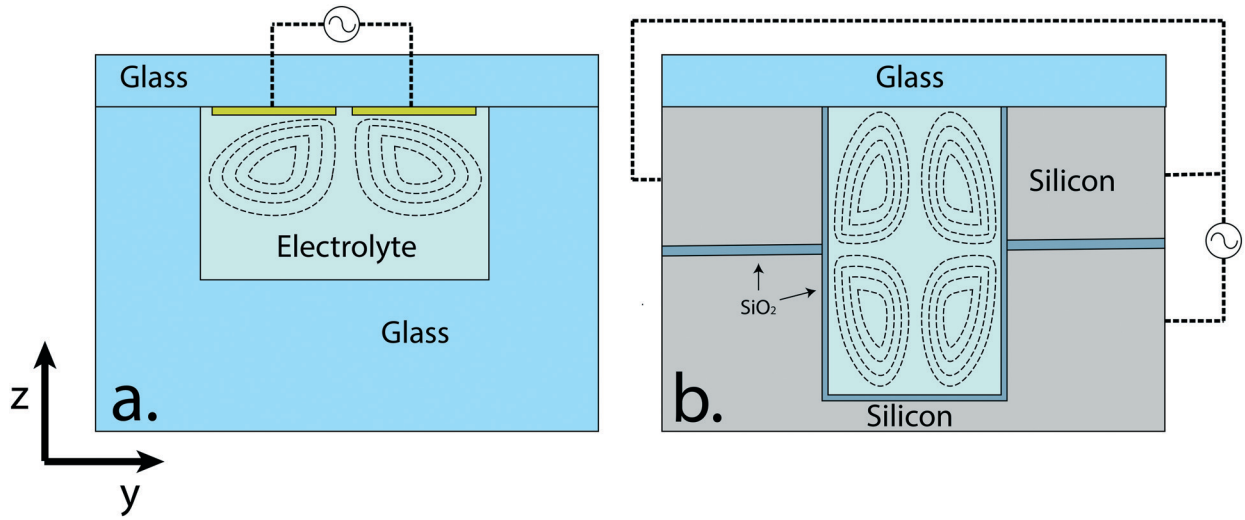


**Fig. 3** AC-electroosmotic flow configurations a) cross-sectional view of the co-planar approach for IC AC-EOF with horizontally oriented (metal) electrodes, b) cross-sectional view of the vertically integrated (doped Si) electrodes, separated by a $SiO_2$ layer. Dotted lines represent the flow lines due to AC-electroosmotic flow.

electrochemically degraded. To avoid such direct contact, a thin insulation layer can be applied. In the present work, we use silicon electrodes where a silicon oxide layer was provided by thermal oxidation. Though the resulting electrolyte-oxide-semiconductor (EOS) system has been extensively studied, *e.g.* in the field of ISFETs, to our knowledge no work has been reported that uses an EOS system to induce AC-EOF.[30–32] The protective oxide layer should be as thin as possible (~10 nm) to maximize the capacity and hence the induced charge in the diffuse double layer, but on the other hand sufficiently thick to avoid pin-holes that result in local leakage currents. When the thickness of the double layer is of a similar magnitude as the oxide layer, the much lower relative permittivity of $SiO_2$ compared to that of water (3.9 *versus* 78) will cause the oxide layer to predominantly determine the charging capacity of the system.

Traditionally, electrodes for AC-EOF are placed in co-planar configurations (see Fig. 3a), with the bare electrodes deposited on a (reversibly bonded) glass cover. This configuration has several disadvantages for applications in chromatography.

Firstly, in this configuration the top substrate with electrodes needs to be aligned and fit into the channel recess before subsequent bonding, which makes the method not suitable when the channels are scaled down to the micrometer regime needed for chromatography.

A more fundamental drawback of the co-planar approach, when aiming for a breakthrough in demanding applications such as chromatography, is that the longest dimension is in-plane with the substrate, limiting the channel volume per area. In the layout presented here on the other hand, the longest dimension is out-of-plane, increasing the total amount of channel volume on the same area, which is critical when parallelizing the system. Furthermore, with the conventional approach, the metal electrodes cannot be functionalized with a chromatographic coating, which creates an additional source of dispersion. Fig. 3b shows the proposed design. Instead of integrating metal electrodes, we use (doped) Si electrodes formed by the Si parts at both sides of a so-called SOI (silicon-on-insulator) substrate. By changing the depth and the thickness of the buried oxide layer as well as the dimensions of the channel, the properties of the device can be adjusted as it provides freedom in the position where the flows (vortices) are induced. Since the chip was made from a SOI wafer, the layered structure is conveniently present in all channels, when etching sufficiently deep. The EOF magnitude is expected to be highest near the electrode gap where the electrical field is highest. Therefore, it is preferable to place this site of maximal lateral speed in the vertical center of the channel, since this will most strongly reduce dispersion. Since the oxide layer is present in the entire chip, the induced AC-potential induces a flow along the entire channel length. In future, other conductor-insulator stacks could be used instead of the Si–SiO stack used here. It has been reported that the 3D geometry of channel and electrodes, and especially the relative length of the electrodes affects the EOF. Olesen *et al.* reported that the confinement of the electric field influences the maximum pumping velocity in their AC-electroosmotic micropump, as well as the frequency at which the pumping velocity was at its maximum.[33] The authors described the level of confinement by $L/H$, where $L$ is the length of the electrode array and $H$ is the height of the channel. Translating this to the system used in this work, $L$ is the wetted perimeter and $H$ half the channel width. The $L/H$ ratio in the system would then be 5, which makes the confinement of limited influence, resulting in an increase of the pumping velocity with a factor of 1.1. However, when we would change the aspect ratio (height/width) of the channel from

AR = 1/4 to AR = 4, the $L/H$ ratio would become in the order of $10^1$. Such an increase to an $L/H$ ratio is expected to increase the maximum pumping velocity with a factor of 1.5.[33] Bazant *et al.* later also realized that the field strength is influenced by geometry.[34]

To determine the electrochemical stability of our system, two parallel streams of an electrolyte solution and an electrolyte solution with added fluorescent dye were introduced while an AC-potential was applied to the silicon electrodes over the course of an hour. During this hour, no change in mixing performance was observed (Fig. S2†), indicating no deterioration of the electrodes. At low frequencies (<8 kHz), the intensity of the fluorescent signal of fluorescein however decreased (Fig. S3†). Since fluorescein is a pH sensitive dye which does not fluoresce at pH < 6.5, this indicates the occurrence of electrochemical reactions at the electrode–electrolyte interface that produce $H^+$, in agreement with what was has been reported for gold electrodes.[35] At the higher frequencies however, no reduction of the fluorescence was observed.

## Flow characterization

To study the AC-EOF flow organization, 3D particle image tracking experiments were performed at 600 mV, lower than the voltages used in the dispersion experiments, as we found that at applied potentials above 1 V the particles became irreversibly adsorbed at the electrode gap, possibly by dielectrophoresis or other electrokinetic effects.[36]

Fig. 4a displays the mean of the magnitude and the direction of the particle velocity for different positions in the cross-section of the channel. The maximum lateral median speed found was 40 μm $s^{-1}$. Two vortices located at both sides of the insulating layers can be observed at the walls of the channel, with the highest magnitude located at the electrode gap. This pattern is consistent with what can be expected from a classic AC-EOF coplanar set-up, since the electric field is of highest magnitude at the point where the distance between the electrodes is the smallest.[37] The vortices at each side are slightly asymmetrical, which we ascribe

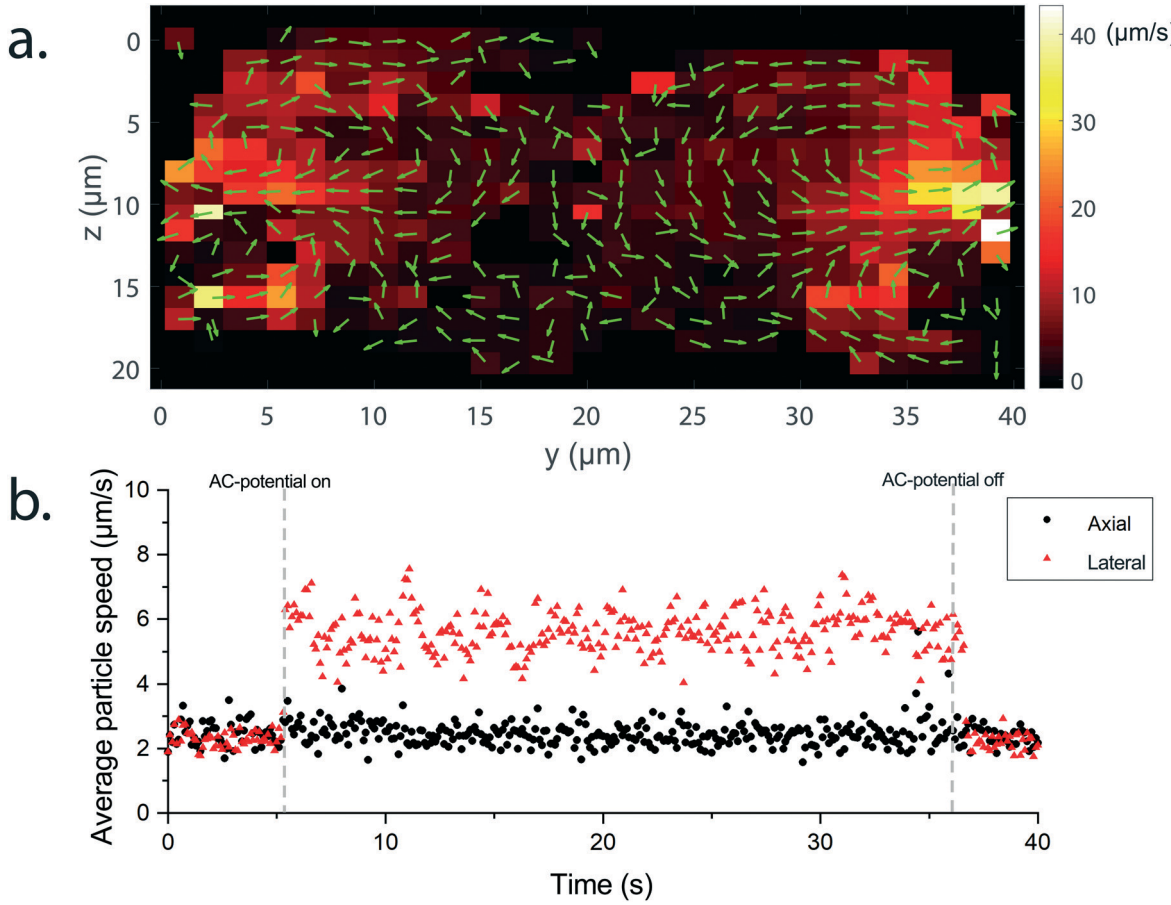


**Fig. 4** Lateral flow characterization. a) Cross-sectional schematic of the microfluidic device, with experimental data from particle tracking velocimetry plotted obtained in a 40 × 20 μm channel at an AC-potential of 600 mV-pp at 10 kHz. The magnitude of the median of the measured particle velocity is displayed as well as the direction. The maximum displayed lateral fluid speed is 40 μm $s^{-1}$ (yellow). Arrows have been normalized. The positions where no measurements were obtained are black without a vector. b) The average particle speed of the detected particles in the channel, in axial and lateral direction *versus* time. There is an increase in the speed in lateral direction when applying an AC-potential, while the speed in axial direction is not influenced. No axial flow was applied, the chip was actuated at 600 mV-pp at 10 kHz. The measurement was performed over a length of 328 μm.

to the asymmetry in the electrode configuration as the top of the channel is formed by an insulating glass wafer where no AC-EOF is generated, while the bottom of the channel is electrode material. As the doped silicon is highly conductive and assuming the oxide layer is of a constant thickness, the charge distribution in the axial direction is uniform and the electroosmotic flow does not have an axial component, since $E_t$ will be zero in axial direction. Fig. 4b shows the axial and lateral speed of polystyrene particles determined over time before, during and after AC-actuation of the chip. As no axial flow was applied, the average velocity before and after AC-actuation is equal in both directions due to Brownian motion. When the AC-actuation is applied, a sudden increase in the average lateral particle velocity magnitude is observed, while there is no change in the axial particle velocity magnitude.

### Reduction of Taylor–Aris dispersion by mixing

To demonstrate that the designed set-up was able to reduce dispersion, we applied AC actuation in a 40 × 20 μm ($w \times h$) microchannel with a buried oxide layer at a depth of 10 μm. The broadening of solute plugs under influence of an axially applied pressure driven flow was monitored. Fig. 5 shows plugs of FITC-dextran in an aqueous solution, shortly after injection into the axial pressure-driven flow. In Fig. 5a, where AC actuation is applied, the plug retains a symmetrical shape, associated with purely longitudinal diffusion, while the plug shown in Fig. 5b assumes a parabolic shape, associated with Taylor dispersion.

To quantitatively express the reduction in Taylor–Aris dispersion, we determined the plate height for both cases (the increase in the plug width variance per length of channel as

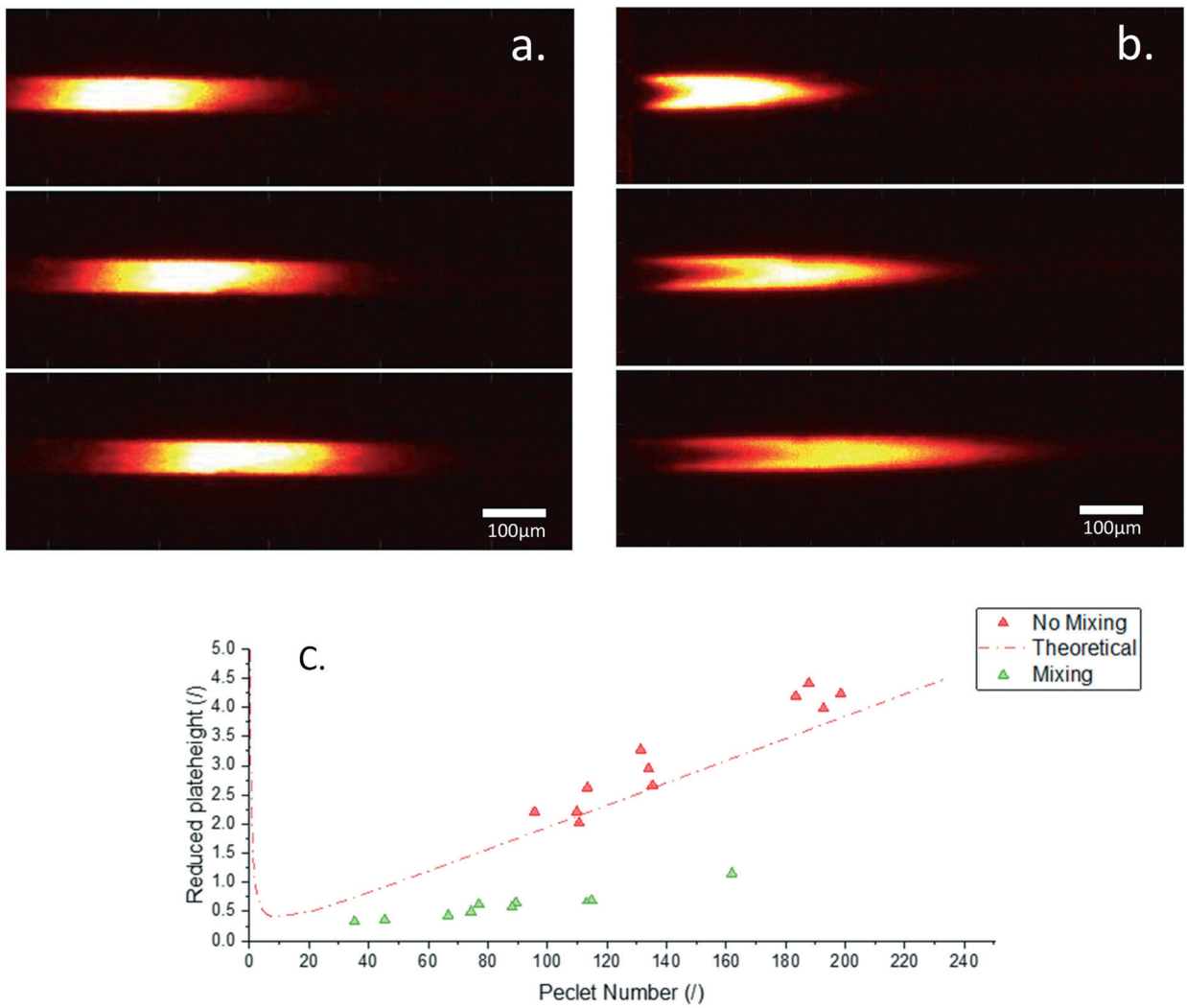


**Fig. 5** Dispersion of FITC-dextran a) fluorescent intensity of an injected plug of FITC-dextran (20 kDa) subject to pressure driven flow with an induced lateral AC-EOF the AC-potential was applied right after the injection was performed. b) Fluorescent intensity of an injected plug of FITC-dextran (20 kDa) subject to pressure driven flow without an induced lateral flow. c) Reduced plate height values at different axial Peclet numbers, with and without lateral mixing. The theoretical plate height is displayed for a channel with aspect ratio 2. Experiments were performed with FITC-dextran 20 kDa, the applied voltage was 10 V-pp at 10 kHz.

formulated in eqn (1)). Fig. 5c shows the reduced plate height, $h = (\Delta\sigma_x^2)/l$, where $\Delta\sigma_x^2$ is the difference in variance at the upstream and downstream measurement positions and $l$ the distance between the two measurement positions. The dimensionless plate height is plotted against the axial Peclet number. In Fig. 5c it can be observed that the experimental results without electroosmotic flow are in agreement with the theoretically predicted plate height values. From these experiments we calculated that for FITC-dextran (20 kDa, $D_m$ = 80 $\mu m^2\ s^{-1}$) the dispersion coefficient ($\kappa_{aris}$) was reduced with a factor of three by inducing a lateral flow, compared to the dispersion without a secondary flow, from $\kappa_{aris}$ = 0.011 to $\kappa_{aris}$ = 0.0035.[38]

This experiment clearly shows that induced lateral vortex flows can strongly reduce Taylor–Aris dispersion. It was performed under non-retained conditions in channels with a relatively large cross section compared to typical chromatographic columns, hence with a low specific surface. To conduct chromatographic separations, the specific surface of the channel should be increased and subsequently coated, and the channel size should be reduced to the micron range to be competitive in absolute numbers of separation performance. With chromatography coatings being only several nanometers thick, the current set-up is expected to still induce an electrohydrodynamic flow when coated. At present the 20 kDa FITC-dextran was used. In protein separations, proteins with weights above 100 kDa are commonly separated.[39,40] These compounds would benefit even benefit more from the increase in mass-transport than the FITC-dextran.

The present design could be combined with well-established methods for the production of pillar arrays, with a spacing ranging from 200 nm up to several μm. As the electrode is composed of Si, the design can also straightforwardly be combined with electrochemical anodization methods, to increase the specific surface.[9,41,42]

Considering downscaling the structure, a decreasing channel spacing is expected to increase the average lateral EOF magnitude as the level of confinement of the electric field increases as well as the average distance between electrodes. The average velocity in the channel will also increase as the ratio distance between the two surfaces at which slip flow is induced, decreases.

### Separation under application of AC-electroosmotic flow

Fig. 6 displays how the reduction in Taylor–Aris dispersion can be used to improve separations. An octadecyltrimethoxysilane (C18) reverse-phase chromatographic coating was applied on the channel wall, using the procedure described in the materials and methods section.[43] Directly after the injection of an analyte plug containing coumarin 440 and 480, an AC-potential was applied inducing AC-EOF. In Fig. 6 it can be observed that the peaks overlapped in the absence of AC-EOF and that the overlap disappeared when AC-EOF was applied. As a result, the resolution was improved with a factor of 1.6. Since coumarin 440 and 480 both have relatively high diffusion coefficients of respectively $4.38 \times 10^{-10}\ m^2\ s^{-1}$ and $3.09 \times 10^{-10}\ m^2\ s^{-1}$,[44] the beneficial effect of the mixing is expected to increase for separations of slower diffusing species (*e.g.* proteins). Future work will focus on further downscaling the device to channel sizes in the micron range,[8,42] which will lead to a higher surface area–volume ratio, therewith increasing retention. Furthermore, as traditionally surfaces are made porous for chromatographic applications to increase the amount of surface area, future work will focus on the ability to induce AC-EOF using porous electrodes.

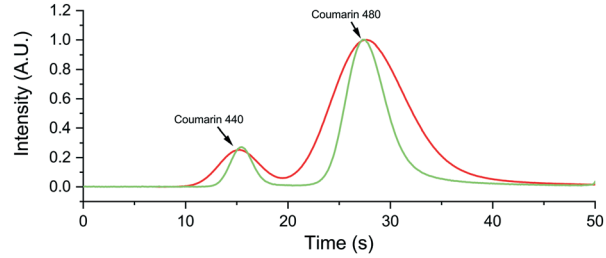


**Fig. 6** Chromatographic separation of coumarin 440 & 480 fluorescence intensity over time without AC-electroosmotic flow (red) and with electroosmotic flow (green). The mixture injected contained coumarin 440 and coumarin 480. The point of analysis was 2 mm downstream from the point of injection.

## Conclusions

In this work we provided a method to actively reduce the Taylor–Aris dispersion in microfluidic channels by using an AC-electroosmotic flow with a new type of micromixer using oxide-insulated electrodes. We demonstrated that Taylor–Aris dispersion coefficient was reduced with a factor of 3 in a channel with a characteristic dimension as small as 20 μm. The reduction was obtained at different axial velocities and decreased the plate height under the theoretical limit in the absence of AC-EOF. Furthermore, we demonstrated the concept of improving chromatographic separations by inducing a lateral flow, by separating two coumarins.

## Conflicts of interest

There are no conflicts of interest to declare.

## Acknowledgements

WDM and EYW greatly acknowledge the European Research Council for the support through the ERC Starting Grant EVODIS (grant number 679033EVODIS ERC-2015-STG). The authors would like to thank Prof. Itzchak Frankel for sharing his insights and for very fruitful discussions.

## Notes and references

1 G. I. Taylor, Dispersion of soluble matter in solvent flowing slowly through a tube, *Proc. R. Soc. London, Ser. A*, 1953, **219**, 186–203.

2 R. A. Aris, On the dispersion of a solute in a fluid flowing through a tube, *Process Syst. Eng.*, 1999, **1**, 109–120.
3 J. L. Dores-Sousa, J. De Vos and S. Eeltink, Resolving power in liquid chromatography: A trade-off between efficiency and analysis time, *J. Sep. Sci.*, 2019, **42**, 38–50.
4 M. Callewaert, W. De Malsche, H. Ottevaere, H. Thienpont and G. Desmet, Assessment and numerical search for minimal taylor-aris dispersion in micro-machined channels of nearly rectangular cross-section, *J. Chromatogr. A*, 2014, **1368**, 70–81.
5 S. A. Khan, A. Günther, M. A. Schmidt and K. F. Jensen, Microfluidic synthesis of colloidal silica, *Langmuir*, 2004, **20**, 8604–8611.
6 A. Tripathi, O. Bozkurt and A. Chauhan, Dispersion in microchannels with temporal temperature variations, *Phys. Fluids*, 2005, **17**, 103607.
7 T. M. Squires and S. R. Quake, Microfluidics: Fluid physics at the nanoliter scale, *Rev. Mod. Phys.*, 2005, **77**, 977–1026.
8 W. De Malsche, *et al.* Pressure-driven reverse-phase liquid chromatography separations in ordered nonporous pillar array columns, *Anal. Chem.*, 2007, **79**, 5915–5926.
9 W. De Malsche, *et al.* Integration of porous layers in ordered pillar arrays for liquid chromatography, *Lab Chip*, 2007, **7**, 1705–1711.
10 W. Malsche, *et al.* Separations using a porous-shell pillar array column on a capillary LC instrument, *J. Sep. Sci.*, 2012, **35**, 2010–2017.
11 K. Broeckhoven, D. Cabooter, S. Eeltink and G. Desmet, Kinetic plot based comparison of the efficiency and peak capacity of high-performance liquid chromatography columns: Theoretical background and selected examples, *J. Chromatogr. A*, 2012, **1228**, 20–30.
12 G. Desmet, D. Clicq and P. Gzil, Geometry-independent plate height representation methods for the direct comparison of the kinetic performance of LC supports with a different size or morphology, *Anal. Chem.*, 2005, **77**, 4058–4070.
13 H. Poppe, Mass transfer in rectangular chromatographic channels, *J. Chromatogr. A*, 2002, **948**, 3–17.
14 D. Dutta and D. T. Leighton, Dispersion in large aspect ratio microchannels for open-channel liquid chromatography, *Anal. Chem.*, 2003, **75**, 57–70.
15 A. D. Stroock, *et al.* Chaotic mixer for microchannels, *Science*, 2002, **295**, 647–651.
16 R. Munirathinam, J. Huskens and W. Verboom, Supported catalysis in continuous-flow microreactors, *Adv. Synth. Catal.*, 2015, **357**, 1093–1123.
17 J. Calvin Giddings, W. A. Manwaring and M. N. Myers, Turbulent-gas chromatography, *Science*, 1966, **154**, 146–148.
18 P. Hajiani and F. Larachi, Reducing Taylor dispersion in capillary laminar flows using magnetically excited nanoparticles: Nanomixing mechanism for micro/nanoscale applications, *Chem. Eng. J.*, 2012, **203**, 492–498.
19 H. Zhao and H. H. Bau, Effect of secondary flows on Taylor-Aris dispersion, *Anal. Chem.*, 2007, **79**, 7792–7798.
20 P. Gelin, Ö. Sardan Sukas, K. Hellemans, D. Maes and W. De Malsche, Study on the mixing and migration behavior of micron-size particles in acoustofluidics, *Chem. Eng. J.*, 2019, **369**, 370–375.
21 R. Barnkob, P. Augustsson, T. Laurell and H. Bruus, Acoustic radiation- and streaming-induced microparticle velocities determined by microparticle image velocimetry in an ultrasound symmetry plane, *Phys. Rev. E: Stat., Nonlinear, Soft Matter Phys.*, 2012, **86**, 056307.
22 S. M. Hagsäter, *et al.* Acoustic resonances in straight micro channels: Beyond the 1D-approximation, *Lab Chip*, 2008, **8**, 1178–1184.
23 D. Ross, T. J. Johnson and L. E. Locascio, Imaging of electroosmotic flow in plastic microchannels, *Anal. Chem.*, 2001, **73**, 2509–2515.
24 S. De Smet and F. Lynen, Kinetic performance evaluation and perspectives of contemporary packed column capillary electrochromatography, *J. Chromatogr. A*, 2014, **1355**, 261–268.
25 M. Baca, *et al.* Performance of laterally elongated pillar array columns in capillary electrochromatography mode, *Electrophoresis*, 2020, 1–9, DOI: 10.1002/elps.202000001.
26 N. G. Green, A. Ramos, A. González, H. Morgan and A. Castellanos, Fluid flow induced by nonuniform ac electric fields in electrolytes on microelectrodes, I. Experimental measurements, *Phys. Rev. E: Stat. Phys., Plasmas, Fluids, Relat. Interdiscip. Top.*, 2000, **61**, 4011–4018.
27 W. De Malsche, E. Westerbeek, J. Eijkel and W. Olthuis, On-chip Structured Silicon-on-Insulator Vortex Inducer, 2020.
28 R. Barnkob, C. J. Kähler and M. Rossi, General defocusing particle tracking, *Lab Chip*, 2015, **15**, 3556–3560.
29 A. González, A. Ramos, N. G. Green, A. Castellanos and H. Morgan, Fluid flow induced by nonuniform ac electric fields in electrolytes on microelectrodes. II. A linear double-layer analysis, *Phys. Rev. E: Stat. Phys., Plasmas, Fluids, Relat. Interdiscip. Top.*, 2000, **61**, 4019–4028.
30 L. Bousse and P. Bergveld, On the impedance of the silicon dioxide/electrolyte interface, *J. Electroanal. Chem. Interfacial Electrochem.*, 1983, **152**, 25–39.
31 P. Schmuki, In Situ Characterization of Anodic Silicon Oxide Films by AC Impedance Measurements, *J. Electrochem. Soc.*, 1995, **142**, 1705.
32 M. S. Kim, *et al.* In-situ monitoring of anodic oxidation of p-type Si(100) by electrochemical impedance techniques in nonaqueous and aqueous solutions, *Bull. Korean Chem. Soc.*, 1999, **20**, 1049–1055.
33 L. H. Olesen, H. Bruus and A. Ajdari, Ac electrokinetic micropumps: The effect of geometrical confinement, Faradaic current injection, and nonlinear surface capacitance, *Phys. Rev. E: Stat., Nonlinear, Soft Matter Phys.*, 2006, **73**, 1–16.
34 M. Z. Bazant and Y. Ben, Theoretical prediction of fast 3D AC electro-osmotic pumps, *Lab Chip*, 2006, **6**, 1455–1461.
35 A. Survila, Electrochemical Processes in Real Systems, *Electrochem. Met. Complexes*, 2015, pp. 115–181, DOI: 10.1002/9783527691241.ch8.
36 S. C. Bukosky, *et al.* Bifurcation in the Steady-State Height of Colloidal Particles near an Electrode in Oscillatory Electric Fields: Evidence for a Tertiary Potential Minimum, *Phys. Rev. X*, 2015, **5**, 1–11.

37 A. Ramos, H. Morgan, N. G. Green and A. Castellanos, Ac electrokinetics: a review of forces in microelectrode structures Dielectrophoretic investigations of sub- micrometre latex spheres N G Green and H Morgan - Ac electrokinetics: a survey of sub- micrometre particle dynamics, *J. Phys. D: Appl. Phys.*, 1998, **31**, 2338–2353.
38 F. Brandl, *et al.* Hydrogel-based drug delivery systems: Comparison of drug diffusivity and release kinetics, *J. Controlled Release*, 2010, **142**, 221–228.
39 K. K. Unger, R. Ditz, E. Machtejevas and R. Skudas, Liquid chromatography-its development and key role in life science applications, *Angew. Chem., Int. Ed.*, 2010, **49**, 2300–2312.
40 P. Benigni, *et al.* Towards the analysis of high molecular weight proteins and protein complexes using TIMS-MS, *Int. J. Ion Mobility Spectrom.*, 2016, **19**, 95–104.
41 J. Op De Beeck, W. De Malsche, P. De Moor and G. Desmet, Hydrodynamic chromatography separations in micro- and nanopillar arrays produced using deep-UV lithography, *J. Sep. Sci.*, 2012, **35**, 1877–1883.
42 W. De Malsche, H. Gardeniers and G. Desmet, Experimental Study of Porous Silicon Shell Pillars under Retentive Conditions Experimental Study of Porous Silicon Shell Pillars, *Anal. Chem.*, 2008, **80**, 5391–5400.
43 M. Baca, G. Desmet, H. Ottevaere and W. De Malsche, Achieving a Peak Capacity of 1800 Using an 8 m Long Pillar Array Column, *Anal. Chem.*, 2019, **91**, 10932–10936.
44 K. Pappaert, J. Biesemans, D. Clicq, S. Vankrunkelsven and G. Desmet, Measurements of diffusion coefficients in 1-D micro- and nanochannels using shear-driven flows, *Lab Chip*, 2005, **5**, 1104–1110.